Non-Aqueous Atomic Layer Deposition of SnO2 for Gas Sensing Application

Catherine Marichy, Ricardo Manuel Silva, N. Pinna, M-G. Willinger, Nicola Donato, Giovanni Neri

Non-Aqueous Atomic Layer Deposition of SnO_2 for Gas Sensing Application

C. Marichy[a], R. M. Silva[b], N. Pinna[c], M-G. Willinger[d], N. Donato[e], G. Neri[e]

[a]Univ Lyon, Université Claude Bernard Lyon 1, CNRS, Laboratoire des Multimatériaux et Interfaces, F-69622 Villeurbanne, France
[b]CICECO - Aveiro Institute of Materials, Department of Materials and Ceramic Engineering, University of Aveiro, Portugal.
[c]Humboldt-Universität zu Berlin, Institut für Chemie, Brook-Taylor-Str. 2 12489 Berlin, Germany.
[d]Scientific Center for Optical and Electron Microscopy (ScopeM), ETH Zürich, Auguste-Piccard-Hof 1, Zürich, Switzerland.
[e]Department of Engineering, University of Messina, Contrada di Dio, Vill. S. Agata, 98166, Messina, Italy.

Tin dioxide thin films are grown at low-moderate temperature using a non-hydrolytic atomic layer deposition process. Granular SnO_2 thin films are obtained from tin(IV) tetra-butoxide reacting with acetic acid, at temperatures as low as 75 °C. Influence of pulse length of both reactants and of the deposition temperature on the saturation is studied. A narrow ALD window is established between 150 and 175 °C with a growth per cycle of 0.07 nm and with a linear growth as a function of the number of cycles. Above 200 °C decomposition of the tin precursor is not negligible. Microstructure and morphology of the as-prepared films as well as the influence of the deposition parameters are investigated using electron and atomic force microscopies. The band gap of the obtained films is determined using UV-visible spectroscopy. Finally the use of the SnO_2 coated carbon nanotubes as gas sensing layer is discussed.

Introduction

Tin dioxide thin films have attracted great attention in recent decades due to their high transparency, their n-type semiconductor behavior and their high direct band gap (~3.6 eV at 25 ºC) (1-3). SnO_2 is widely studied for application as transparent conducting oxide, heterogeneous catalyst, Li-ion battery anode and solid-state gas sensor (4). It has proven to be one of the most suited active layer in resistive metal oxide semiconductor (MOS) gas sensors (5). Nonetheless, high operating temperature is often required with such MOS gas sensors, due to their high resistivity. To overcome this issue and decrease the overall resistance of the device, an attractive strategy consists in depositing the metal oxide on a conductive support. In particular, because of their high surface area, good thermal and electric conductivity, and mechanical as well as chemical stability, carbon nanotubes (CNTs) provide ideal properties as a support for a second material that can be deposited onto their surface either as particles or as a thin film. Elaboration of such CNTs coated with SnO_2 required a synthetic approach capable to control the deposition at the atomic scale.

SnO_2 thin films can be deposited onto various substrates by chemical and physical deposition processes (6). Due to its high conformality and homogeneity Atomic Layer Deposition (ALD) is the technique of choice for thin film deposition and it has already been applied to SnO_2 deposition onto various supports (7). In particular, SnO_2 can be deposited from $SnCl_4$ reacting with either water (8-12) or hydrogen peroxide (13-17) or from SnI_4 and either H_2O_2 (14, 16) or O_2 (14, 16-19) at relatively high temperatures (180-700 °C). In order to decrease the deposition temperature, to avoid corrosive by-products and further to obtain amorphous films, alternative strategies have been developed based on metalorganic precursor (20-28). For instance, Gordon et al. reported a low temperature approach based on a cyclic amide precursor reacting with either hydrogen peroxide (29) or NO (30), from 50 to 200 ºC and 130 to 250 ºC, respectively. The very few low temperature SnO_2 ALD processes reported involve in most of the cases oxygen sources with high oxidative power, like oxygen plasma, O_3 and H_2O_2 (7). It is certainly of interest to access SnO_2 by ALD at gentle deposition conditions, especially in view of fabricating CNT based heterostructures. Indeed, strong oxidative reactants might damage the carbon substrates by creating surface defect and oxygenated sites which deteriorate the support intrinsic electronic properties. Simultaneously to Gordon's work, we have introduced a non- hydrolytic ALD process for SnO_2 (31).

Based on the reaction between tin tert-butoxide ($Sn(O^tBu)_4$) and acetic acid, SnO_2 is deposited at low/middle temperature onto various substrates. Especially, CNTs can be efficiently either decorated or coated (31). The present contribution focuses on the systematic study of the ALD parameters of the proposed approach. The film characteristics on flat substrates as well as SnO_2-coated CNT (SnO_2/CNT) heterostructures will also be discussed. Implementation of the present ALD process to gas sensitive layer will be only exemplified here as the reader can refer to previous papers (31, 32) on the gas sensing properties of ALD SnO_2/CNT structures.

Experimental

SnO_2 deposition

Tin dioxide was deposited on Si(100) wafer. Prior deposition the substrates were cleaned with piranha solution for 30 min at 80 ºC, washed thoroughly with distillated water and finally dried with nitrogen. Tin tert-butoxide (99.99% PURATREM, STREM and ≥99.99%, Aldrich) and acetic acid (Purum ≥99.0%, Fluka) were used as metal and oxygen precursors, respectively. Metal precursor and carboxylic acid were introduced subsequently by pneumatic ALD valves from their reservoirs, which were kept at 80 and 20 ºC, respectively. For the deposition, pure nitrogen was used as a carrier gas at a constant flow rate of 5 sccm.

The depositions took place between 75 and 250 °C in an exposure mode reactor with an opening time of 1 s and 0.03 s for the tin and oxygen sources, respectively. Once the ALD window was determined, in order to investigate the growth rate as a function of the various ALD parameters, depositions at 175 °C were realized using opening times ranging from 0.5 to 2 s and 0.02 to 1 s for tin precursor and acetic acid, respectively. The residence time after each precursor pulse was set to 20 s, followed by a nitrogen purge of 15 s.

Deposition of SnO_2 was then carried out on two types of carbon nanotubes, Pyrograph PR-24-PS and PR-24-HHT, having different degrees of graphitization. Both are purchased from Applied Science. Prior ALD, CNTs were functionalized by HNO_3 treatment at 100 °C for 10h. The depositions took place at 200 ºC. ALD valves were opened for 0.03 and 1 s for the acetic acid and tin ter-butoxide, respectively. The residence time after each precursor pulse was set to 20 s, followed by a nitrogen purge during 15 s. The number cycles varied from 50 to 1000.

Characterization of the as-deposited films

The thickness of as-deposited tin oxide films on wafer substrates were measured either by X-ray reflectometry (XRR) or by ellipsometry spectroscopy. XRR was performed using a Philips X'Pert MRD X-ray diffractometer with copper radiation and a graphite monochromator for the selection of pure Kα radiation. The X-ray tube was operated at 40 kV and 50 mA. A 1 mm slit was used in order to reduce the scattered X-ray intensity. Measurements were performed in low-resolution experimental set up with the following instrumental configuration: divergence slit at the incident beam: 1/8 in.; step width: 0.005°; acquisition time: 1 s. Ellipsometry spectroscopy was realized at an incidence angle of 70° with a detector set at 45° using a Sopra ellipso-porosimeter. Data fit was realized with "Winell II" software using Cauchy dispersion law. Coated wafers were further analyzed by scanning electron microscopy (SEM) and energy dispersive spectroscopy (EDS) using a SU-70 (Hitachi) microscope equipped with a Bruker silicon drift detector. The surface morphology was studied by atomic force microscopy (AFM) in tapping mode using a commercial Bruker MFP-3D Asylum microscope with a resonant frequency of 1.5Hz. UV-visible absorption spectra were recorded at room temperature, using a dual beam spectrophotometer Lambda 950, Perkin Elmer, with a 150 nm diameter integrating sphere.

Result and discussion

ALD parameters

Considering that tin tert-butoxide has a boiling point at 65 °C under 0.3 torr and that the working pressure of the ALD chamber is 0.1 torr, the metal source canister temperature is set at 80 °C to ensure its vaporization. The SnO_2 growth rate on Si(100) with OH surface groups is first evaluated in the range of 75-250 °C; Figure 1 shows the obtained growth per cycle (GPC) as a function of the deposition temperature. Tin dioxide films can be deposited at temperature as low as 75 °C, despite a low GPC of 0.03 nm/cycle. No attempt is realized below this temperature because of the risk of Sn precursor condensation and film contamination by remaining physisorbed carboxylic acid on ALD chamber wall. With a GPC value around 0.07 nm/cycle, a relatively steady regime between 150 and 175 °C, which can even be extended up to 200 °C (GPC between 0.07 – 0.08 nm/cycle) is obtained. Above 200 °C, a significant increase of the GPC is visible probably correlated to the beginning of tin precursor decomposition by β-hydride elimination.

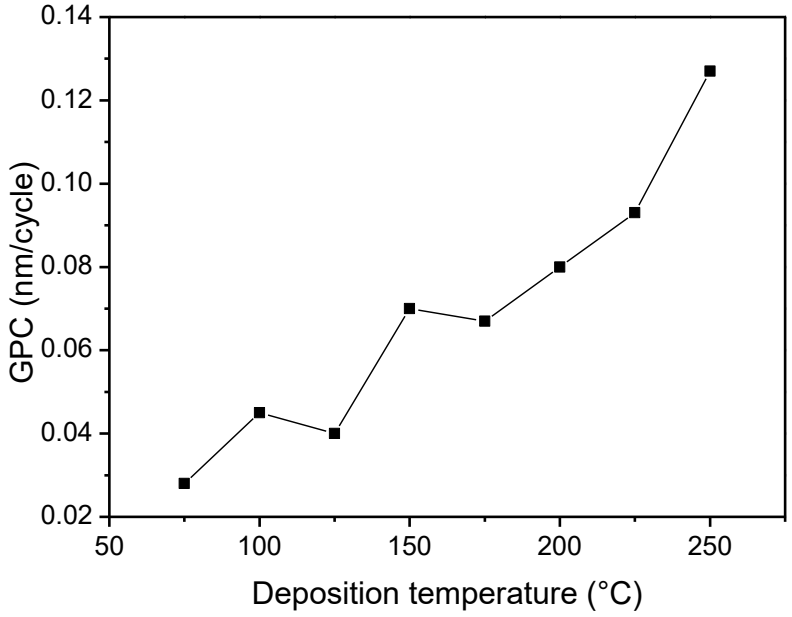

Figure 1. GPC of SnO_2 films as a function of the deposition temperature. Acetic acid and Tin(IV) tetra-butoxide pulse lengths were set at 0.03 and 1.0 s, respectively.

To study the self-limiting growth behavior of the process a deposition temperature of 175 °C was selected and the GPC was evaluated as a function of the precursor dosing. Figure 2 reveals that pulses of 1.5 and 0.04 s of tin and oxygen source, respectively, are sufficient to reach the saturation. No significant increase of GPC occurs with longer precursors pulses, demonstrating the completion and self-limiting character of the surface reactions. In the following, to ensure the self-limiting regime, the pulse length of $Sn(O^tBu)_4$ and acetic acid are set at 1.5 and 0.4 s, respectively.

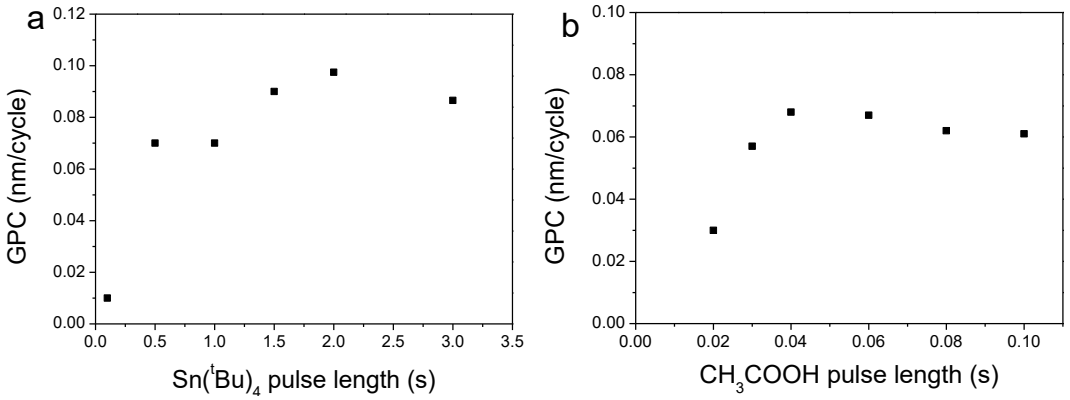

Figure 2. GPC of SnO_2 films as a function of a) $Sn(O^tBu)_4$ pulse length (acetic acid pulse and purge set, respectively, at 0.03 and 15 s) and b) the acetic acid pulse length (Sn precursor pulse and purge set, respectively, at 1.5 and 15 s). The deposition temperature is 175 °C in both cases.

Linear dependence of the film thickness on the number of cycles, which is characteristic of ALD growth, is verified using the optimized parameters (Figure 3). It should be highlighted that extrapolation to the origin indicates a nucleation delay of approximately 10 cycles. Further experiments are required to further study the SnO_2 nucleation behavior during the first cycles.

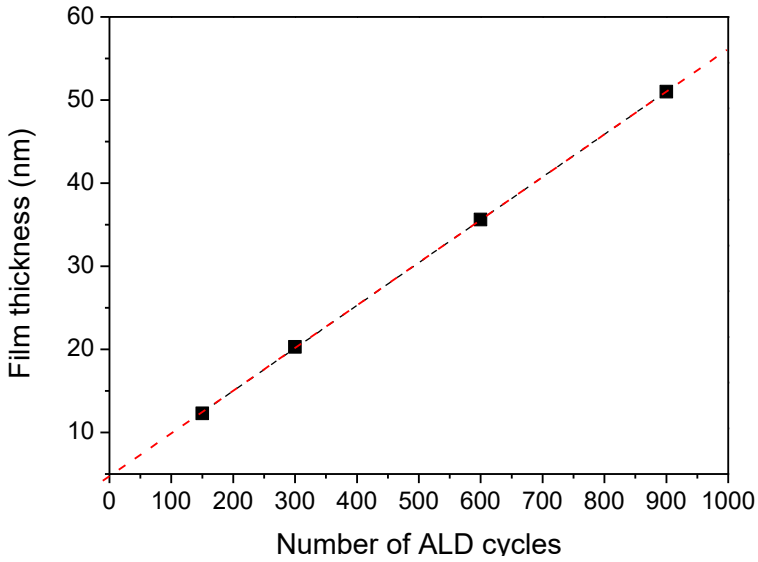

Figure 3. SnO_2 film thickness as a function of the number of ALD cycles.

As-deposited SnO_2 thin films on Si wafer

The obtained films are continuous and homogenous on the whole Si wafer surface. Cross-section SEM image of 120 nm-thick SnO_2 deposit on Si, shown in Figure 4a, evidences the continuity and thickness uniformity of the coating deposited at 200 °C. High magnification SEM imaging (Figure 4b) suggests the presence of small SnO_2 grains and thus a granular morphology of the film. This is in agreement with previous observations on SnO_2 deposited at 200 °C, which have revealed that the oxide coating consists on sub-10 nm polycrystals (31). To investigate the influence of the deposition temperature on the material microstructure, films of approximately 40 nm grown at 100 and 175 °C are characterized by AFM. Figure 4 c,d evidences the granular structure of the as-deposited films, independently of the growth temperature. The size of the particles seems unaffected by the ALD parameter and no significant increase of the root mean square (RMS) roughness is noticed. Therefore, formation of sub-10 nanoparticles seems inherent to the process and the deposited material, as well as independent of the deposition conditions. One can hypothesize that Volmer-Weber growth mode occurs during the non-hydrolytic ALD process. It can be pointed out that such growth has not been reported on V_2O_5 and TiO_2 ALD using acetic acid as oxygen source. They both display typical 2D mode, indeed (33, 34).

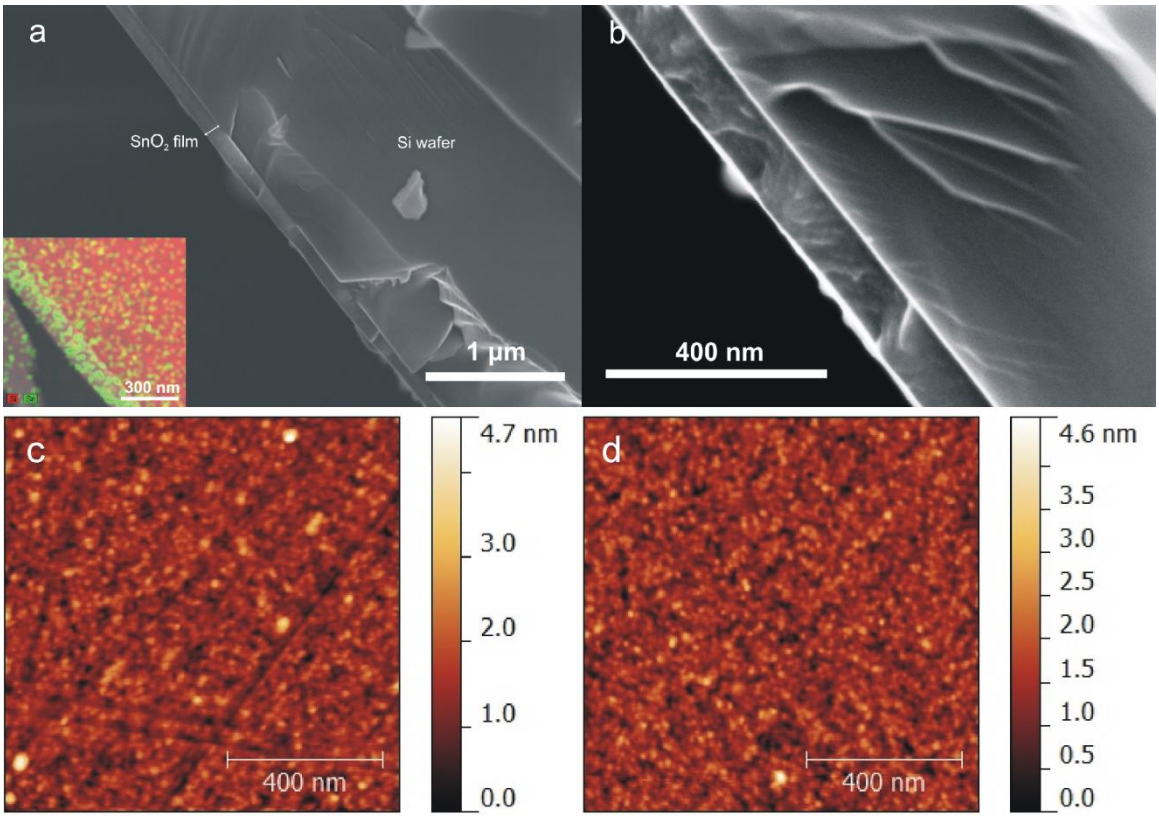

Figure 3. a,b) Cross-section SEM imaging of 120 nm thick SnO_2 film on silicon wafer, a) at low magnification, in inset EDS map shows the presence of film on the side. Si and Sn are represented with red and green code, respectively. b) At higher magnification, the SEM image reveals a granular morphology of the film. c,d) 1x1 µm AFM images of SnO_2 film on Si grown at c) 175 °C (measured RMS=0.416 nm) and d) 100 °C (measured RMS=0.411 nm)

In our previous paper, the formation of high purity SnO_2 films without carbon contamination and constituted of nanocrystal of rutile SnO_2 has been reported (31). Herein, we extend this study to the determination of the band gap, Eg, using UV-Visible reflectance spectroscopy. The reflectance spectra of 30 and 120 nm thick films deposited on Si wafer are shown in Figure 4a. Absorption between 250-400 nm is noted in both cases as well as a decrease of the reflectance for the thicker film. Tin dioxide band gap is expected to be direct. Its value can therefore be obtained graphically by plotting $(F(R)*E)^2$ vs. E, where F(R) is the Kulbelka-Munk function: $F(R) = (1-R)^2/2R$, with R the reflectance value (35). The Eg value is determined at the intersection of the linear fit with the energy axis for 0 coordinate (Figure 4b). Thin films being considered, the support reflectance contribution is preliminary reduced by dividing the measured reflectance spectra of the supported film by reference spectra. For both films (only 120 nm thick SnO_2 shown in Figure 4b), the extracted band gap is 3.4 eV that is realistic although slightly lower than the theoretical value of the bulk (3.6 eV). The nanocrystallinity and probable amorphous phase as well as lower density of the ALD tin dioxide could explain the observed difference between the E_g of the film and the expected one.

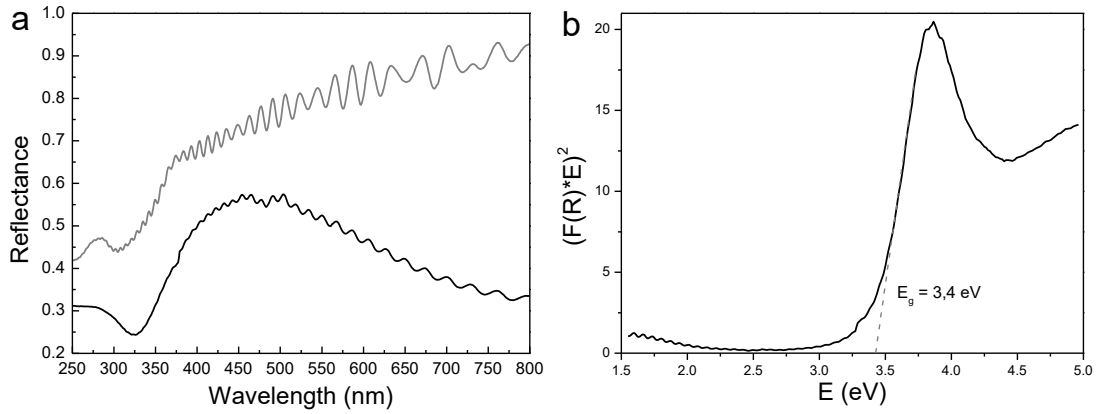

Figure 4. a) UV-Visible reflectance spectra of a 30 nm (grey line) and 120 nm (black line) thick SnO_2 films on Si, after removal of the support contribution. b) Kulbelka-Munk transformed reflectance spectrum and linear fit of the 120 nm SnO_2 thin films.

As-deposited SnO_2 on CNTs

As previously reported, the present ALD approach reveals suited for depositing tin dioxide onto carbon nanotubes (31). Tin dioxide is deposited on two types of cup-stack CNTs: the PR-24-PS CNTs have a pyrolytic carbon layer at their surface and display large density of oxygen anchoring groups after functionalization, while the PR-24-HHT CNTs present highly graphitized walls, with stacked cone connections where few anchoring sites are located after acid treatment (36, 37). Depending on the degree of graphitization of the CNT support and thus density of surface oxygenated species (38), either a continuous coating on the inner and outer walls or a distinct metal oxide decoration is observed, as shown in Figure 5. In particular, relatively homogeneous and smooth film, despite its granular aspect, is obtained on PR-24-PS CNTs (Figure 5a). On the contrary, after 50 cycles, small particles nucleating on the curved graphene sheet between two cones initiate the formation of rings wrapped around the PR-24-HHT CNT (Figure 5b). This particular structure is well observed after 400 cycles (Figure 5c). HRTEM confirms the initiation at the step edge. Indeed, in Figure 5e,f, the arrows clearly point to particles nucleating on defective spots of the tubes. Each of them can be correlated to either an edge or a dip in the graphitized carbon.

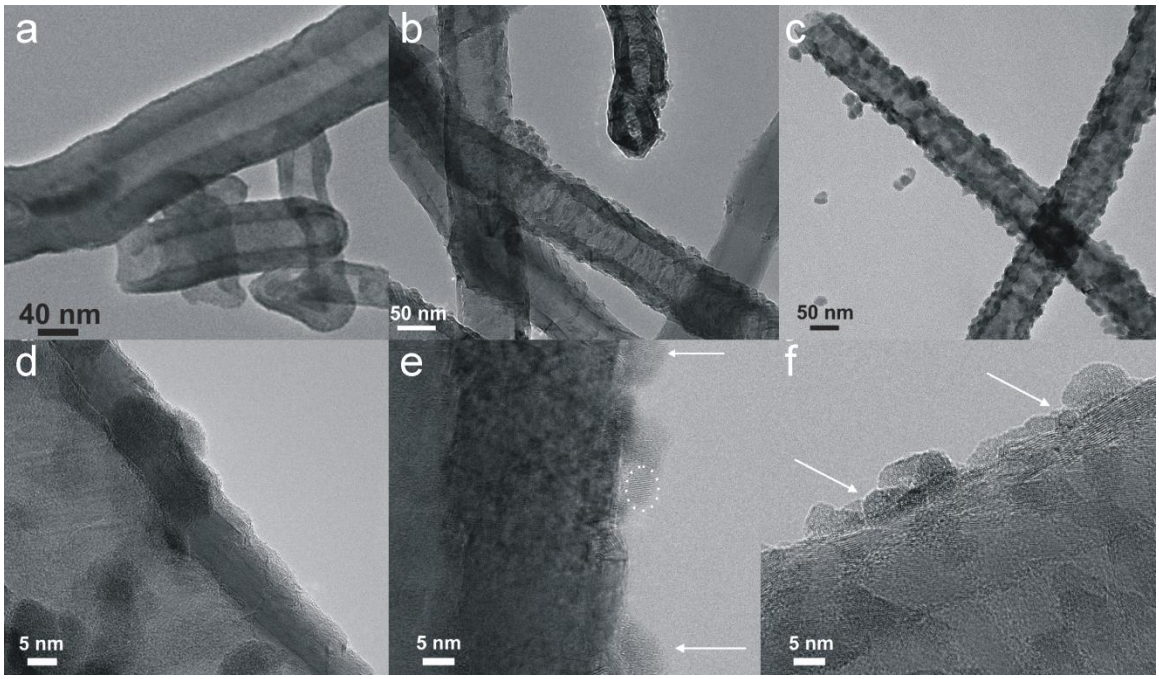

Figure 5. TEM images of a) PR-24-PS CNTs coated with 200 SnO_2 ALD cycles and b,c) PR-24-HHT CNTs decorated with b) 50 and c) 400 SnO_2 cycles. Loose particles, resulting most likely from a mechanical removal, are observed in c). HRTEM images of SnO_2 decorated PR-24-HHT after d) 400cycles, e and f) 50 cycles. The arrows point to some particles nucleating at defect sites and the dotted circle underlines lattice fringes related to SnO_2 rutile phase.

Furthermore, HRTEM images permit to enlighten the presence of SnO_2 in a tetragonal phase. Lattice fringes with plane spacing close of 3.34 Å and 2.67 Å, which are indexed to the crystal planes (110) and (101) of the tetragonal rutile phase (JCPDS card nº 00-001-0625) are nicely observed in Figure 6.

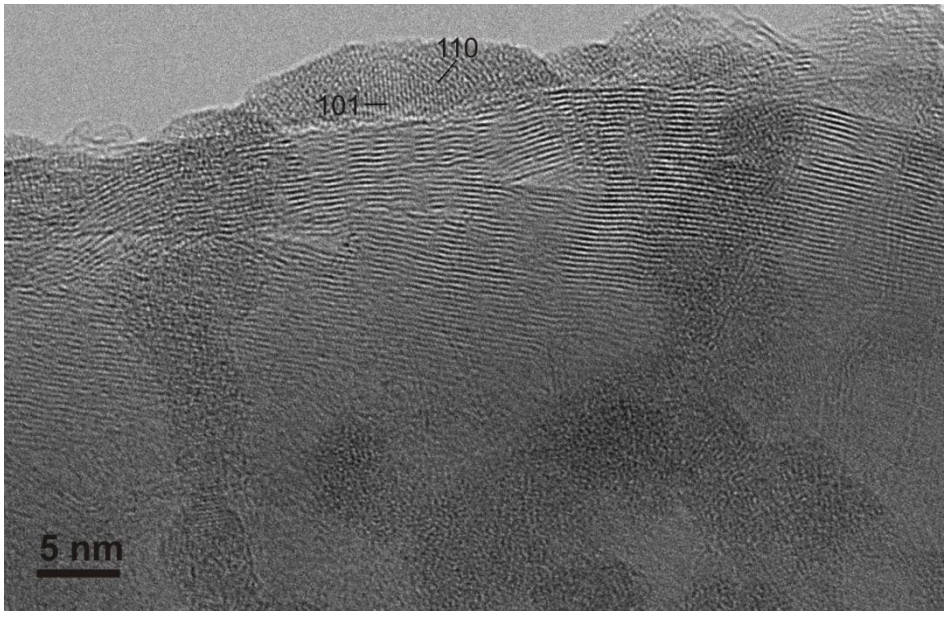

Figure 6. HRTEM of SO_2 decorated PR-24-HHT CNTs after 50 ALD cycles.

Gas Sensing

Finally, the ALD fabricated SnO_2/CNTs heterostructures can be efficiently used as sensitive layers in sensing devices as it has been already reported (31, 32). **Figure 7** exemplifies the sensing properties of 3 nm SnO_2 layer on PR-24-PS CNTs toward NO_2. The transient response to 5 ppm of NO_2 at 150 °C shows a drastic and reversible increase of resistance in presence of the target gas. The response is attributed to the synergy and the p-n heterojunction between both materials (31, 34, 39, 40).

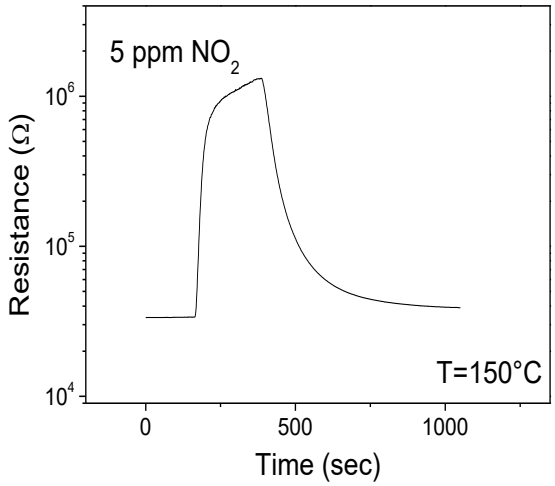

Figure 7. Transient responses of 3.0 nm SnO_2-coated PR-24-PS CNTs to 5 ppm of NO_2 at 150 °C.

Conclusion

The proposed non-aqueous ALD process permits to deposit uniform SnO_2 thin films at temperature as low as 75 °C. A near steady regime with a nominal GPC of 0.07 nm/cycle is noted in the temperature range of 150-175 °C. Saturation of the surface reactions is verified with tin(IV) tert-butoxide and acetic acid pulse lengths of 1.5 and 0.04 s, respectively. The as-deposited films show a granular like structure composed of sub-ten nanometer nanoparticles independently of the deposition temperature. Moreover, the as-deposited SnO_2 presents a bang gap of 3.4 eV, slightly lower than the theoretical band gap of the bulk metal oxide. Finally, SnO_2 films and decorations are effectively formed by ALD on CNT supports, depending on the graphitization degree of the support. The fabricated heterostructures are efficiently applied as sensing layer for NO_2 detection demonstrating the potentiality of the ALD process for gas sensing application.

Acknowledgements

Dr. Rute Ferreira, from the University of Aveiro (Portugal) and A. Piednoir, from the University of Lyon (France) are acknowledged for optical measurements and AFM characterization, respectively. Prof. Jean-Philippe Tessonnier, from Iowa State University(USA), is acknowledged for supplying the two type of functionalized CNTs.

References

1. Barbarat, P.; F. Matar, S.; Le Blevennec, G. *J. Mater. Chem.*,**7** (12), 2547-2550 (1997).
2. Fröhlich, D.; Kenklies, R.; Helbig, R. *Phys. Rev. Lett.*,**41** (25), 1750-1751 (1978).
3. Godinho, K. G.; Walsh, A.; Watson, G. W. *J. Phys. Chem. C*,**113** (1), 439-448 (2009).
4. Batzill, M.; Diebold, U. *Prog. Surf. Sci.*,**79** (2-4), 47-154 (2005).
5. Gopel, W.; Schierbaum, K. D. *Sens. Actuators, B*,**26** (1-3), 1-12 (1995).
6. Sberveglieri, G. *Sens. Actuators, B*,**6** (1â€“3), 239-247 (1992).
7. Nazarov, D. V.; Bobrysheva, N. P.; Osmolovskaya, O. M.; Osmolovsky, M. G.; Smirnov, V. M. *Reviews on Advanced Materials Science*,**40**, 262-275 (2015).
8. Matero, R.; Rahtu, A.; Ritala, M.; Leskelä, M.; Sajavaara, T. *Thin Solid Films*,**368** (1), 1-7 (2000).
9. Takeuchi, T.; Shoji, K.; Tadano, T.; Doteshita, I.; Onodera, S. *Thin Solid Films*,**442** (1-2), 98-101 (2003).
10. Tarre, A.; Rosental, A.; Sammelselg, V.; Uustare, T. *Appl. Surf. Sci.*,**175**, 111-116 (2001).
11. Utriainen, M.; Kovacs, K.; Campbell, J. M.; Niinistö, L.; Reti, F. *J. Electrochem. Soc.*,**146** (1), 189-193 (1999).
12. Viirola, H.; Niinistö, L. *Thin Solid Films*,**249** (2), 144-149 (1994).
13. Du, X.; Du, Y.; George, S. M. *J. Vac. Sci. Technol., A*,**23** (4), 581-588 (2005).
14. Lu, J.; Sundqvist, J.; Ottosson, M.; Tarre, A.; Rosental, A.; Aarik, J.; Harsta, A. *J. Cryst. Growth*,**260** (1-2), 191-200 (2004).
15. Natarajan, G.; Cameron, D. *Appl. Phys. A*,**95** (3), 621-627 (2009).
16. Rosental, A.; Tarre, A.; Gerst, A.; Sundqvist, J.; Harsta, A.; Aidla, A.; Aarik, J.; Sammelselg, V.; Uustare, T. *Sens. Actuators, B*,**93** (1-3), 552-555 (2003).
17. Tarre, A. R., A.; Aidla, A.; Aarik, J.; Sundqvist, J.; Harsta, A. *Vacuum*,**67**, 571-575 (2002).
18. Sundqvist, J.; Lu, J.; Ottosson, M.; Harsta, A. *Thin Solid Films*,**514** (1-2), 63-68 (2006).
19. Tarre, A.; Rosental, A.; Sundqvist, J.; Harsta, A.; Uustare, T.; Sammelselg, V. *Surf. Sci.*,**532**, 514-518 (2003).
20. Drozd, V. E.; Aleskovski, V. B. *Appl. Surf. Sci.*,**82-83**, 591-594 (1994).
21. Choi, G.; Satyanarayana, L.; Park, J. *Appl. Surf. Sci.*,**252** (22), 7878-7883 (2006).
22. Kim, D. H.; Kim, W.-S.; Lee, S. B.; Hong, S.-H. *Sens. Actuators, B*,**147** (2), 653-659 (2010).
23. Kim, D. H.; Kwon, J.-H.; Kim, M.; Hong, S.-H. *J. Cryst. Growth*,**322** (1), 33-37 (2011).
24. Kim, W.-S.; Lee, B.-S.; Kim, D.-H.; Kim, H.-C.; Yu, W.-R.; Hong, S.-H. *Nanotechnology*,**21** (24), 245605-245611 (2010).
25. Lee, W.; Hong, K.; Park, Y.; Kim, N. H.; Choi, Y.; Park, J. *Electron. Lett.*,**41** (8), 475-477 (2005).
26. Choi, W.-S. *Trans. Electr. Electron. Mater.*,**10** (6), 200-202 (2009).
27. Mullings, M. N.; Hägglund, C.; Bent, S. F. *Journal of Vacuum Science & Technology A*,**31** (6), - (2013).
28. Elam, J. W.; Baker, D. A.; Hryn, A. J.; Martinson, A. B. F.; Pellin, M. J.; Hupp, J. T. *J. Vac. Sci. Technol., A*,**26** (2), 244-252 (2008).
29. Heo, J.; Hock, A. S.; Gordon, R. G. *Chem. Mater.*,**22** (17), 4964–4973 (2010).

30. Heo, J.; Kim, S. B.; Gordon, R. G. *J. Mater. Chem.*,**22**, 4599-4602 (2012).
31. Marichy, C.; Donato, N.; Willinger, M.-G.; Latino, M.; Karpinsky, D.; Yu, S.-H.; Neri, G.; Pinna, N. *Adv. Funct. Mater.*,**21** (4), 658-666 (2011).
32. Marichy, C.; Russo, P. A.; Donato, N.; Latino, M.; Neri, G.; Pinna, N. *J. Phys. Chem.*,**117** (38), 19729-19739 (2013).
33. Rauwel, E.; Willinger, M. G.; Ducroquet, F.; Rauwel, P.; Matko, I.; Kiselev, D.; Pinna, N. *J. Phys. Chem. C*,**112** (33), 12754-12759 (2008).
34. Willinger, M. G.; Neri, G.; Rauwel, E.; Bonavita, A.; Micali, G.; Pinna, N. *Nano Lett.*,**8** (12), 4201-4204 (2008).
35. Weber, R. S. *J. Catal.*,**151** (2), 470-474 (1995).
36. Tessonnier, J.-P.; Rosenthal, D.; Girgsdies, F.; Amadou, J.; Begin, D.; Pham-Huu, C.; Sheng Su, D.; Schlögl, R. *Chem. Commun.* (46), 7158-7160 (2009).
37. Tessonnier, J.-P.; Rosenthal, D.; Hansen, T. W.; Hess, C.; Schuster, M. E.; Blume, R.; Girgsdies, F.; Pfänder, N.; Timpe, O.; Su, D. S.; Schlögl, R. *Carbon*,**47** (7), 1779-1798 (2009).
38. Marichy, C.; Tessonnier, J.-P.; Ferro, M. C.; Lee, K.-H.; Schlögl, R.; Pinna, N.; Willinger, M.-G. *J. Mater. Chem.*,**22**, 7323-7330 (2012).
39. Marichy, C.; Russo, P. A.; Latino, M.; Tessonnier, J.-P.; Willinger, M.-G.; Donato, N.; Neri, G.; Pinna, N. *J. Phys. Chem. C*,**117** (38), 19729-19739 (2013).
40. Willinger, M. G.; Neri, G.; Bonavita, A.; Micali, G.; Rauwel, E.; Herntrich, T.; Pinna, N. *Phys. Chem. Chem. Phys.*,**11** (19), 3615-3622 (2009).